Inorganic Chemistry

pubs.acs.org/IC

Article

Green Light-Triggered Photocatalytic Anticancer Activity of Terpyridine-Based Ru(II) Photocatalysts

Arif Ali Mandal, Virendra Singh, Sukanta Saha, Silda Peters, Tumpa Sadhukhan, Rajesh Kushwaha, Ashish Kumar Yadav, Apurba Mandal, Aarti Upadhyay, Arpan Bera,* Arnab Dutta, Biplob Koch,* and Samya Banerjee*

Cite This: *Inorg. Chem.* 2024, 63, 7493−7503

Read Online

ACCESS | Metrics & More | Article Recommendations | Supporting Information

ABSTRACT: The relentless increase in drug resistance of platinum-based chemotherapeutics has opened the scope for other new cancer therapies with novel mechanisms of action (MoA). Recently, photocatalytic cancer therapy, an intrusive catalytic treatment, is receiving significant interest due to its multitargeting cell death mechanism with high selectivity. Here, we report the synthesis and characterization of three photoresponsive Ru(II) complexes, viz., [Ru(ph-tpy)(bpy)Cl]PF_6 (**Ru1**), [Ru(ph-tpy)(phen)Cl]PF_6 (**Ru2**), and [Ru(ph-tpy)(aip)Cl]PF_6 (**Ru3**), where, ph-tpy = 4′-phenyl-2,2′:6′,2″-terpyridine, bpy = 2,2′-bipyridine, phen = 1,10-phenanthroline, and aip = 2-(anthracen-9-yl)-1*H*-imidazo[4,5-*f*][1,10] phenanthroline, showing photocatalytic anticancer activity. The X-ray crystal structures of **Ru1** and **Ru2** revealed a distorted octahedral geometry with a RuN_5Cl core. The complexes showed an intense absorption band in the 440−600 nm range corresponding to the metal-to-ligand charge transfer (MLCT) that was further used to achieve the green light-induced photocatalytic anticancer effect. The mitochondria-targeting photostable complex **Ru3** induced phototoxicity with IC_{50} and PI values of ca. 0.7 μM and 88, respectively, under white light irradiation and ca. 1.9 μM and 35 under green light irradiation against HeLa cells. The complexes (**Ru1**−**Ru3**) showed negligible dark cytotoxicity toward normal splenocytes (IC_{50s} > 50 μM). The cell death mechanistic study revealed that **Ru3** induced ROS-mediated apoptosis in HeLa cells via mitochondrial depolarization under white or green light exposure. Interestingly, **Ru3** also acted as a highly potent catalyst for NADH photo-oxidation under green light. This NADH photo-oxidation process also contributed to the photocytotoxicity of the complexes. Overall, **Ru3** presented multitargeting synergistic type I and type II photochemotherapeutic effects.

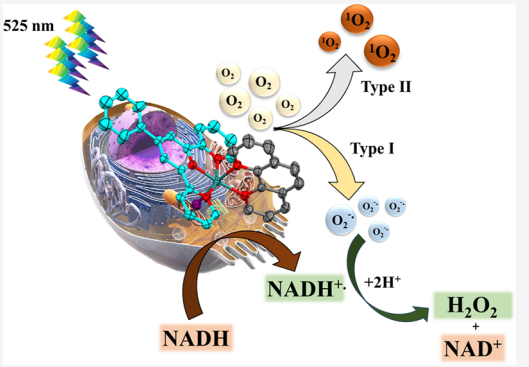

INTRODUCTION

Cancer is one of the major causes of death worldwide (ca. 10 M deaths in 2020) and it is badly affecting the global health index.[1] Primarily, Pt-based anticancer drugs have been employed as chemotherapeutics in combating this disease.[2−5] However, their low tumor selectivity, adverse side effects, and acquired drug resistance have led to new initiatives toward developing better chemotherapeutic agents and advanced cancer therapies with reduced side effects, better tumor selectivity, and enhanced cytotoxicity.[6,7] Recently, a new type of photoactivated cancer therapy termed "photocatalytic cancer therapy" has arisen as a potential non-invasive alternative to the current cancer therapies.[8−11] In photocatalytic cancer therapy, a photosensitive drug molecule is exposed to a certain wavelength of light to induce cytotoxicity via in-cell catalytic reactions and the production of reactive oxygen species (ROS).[12−15] The in-cell catalytic reactions (such as NADH/NAD(P)H oxidation) and ROS generation are ultimately reported to perturb energy metabolism and redox state in cancer cells selectively.[10,16] These further disrupt cell signaling cascades and/or modify gene expression regulation, ultimately causing tumor cell damage.[17−19] This novel concept, photocatalytic cancer therapy, has shown promising results in overcoming cisplatin resistance with high tumor selectivity both *in vivo* and *in vitro*.[20] The advantages of photocatalytic cancer drug development could be (i) low to extremely low drug dose, helpful to avoid the toxicity of metal (in the case of metal-based photocatalytic anticancer agents), (ii) selective activation of the drug at the specified tumor site, helpful to reduce drug's side effects, and (iii) overcoming current drug resistance issues by multifunctional and multitargeting anticancer mechanism.[21,22]

Received: February 14, 2024
Revised: March 25, 2024
Accepted: March 25, 2024
Published: April 5, 2024

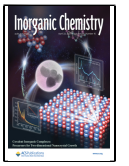

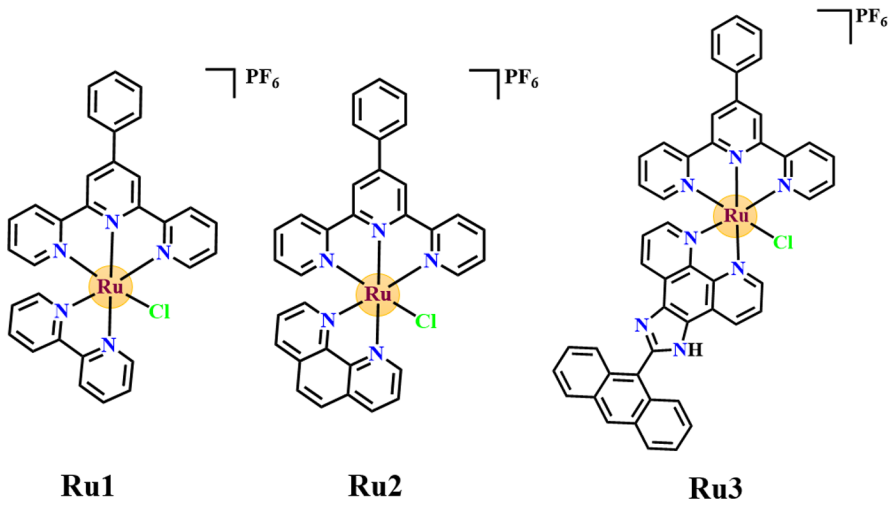

Figure 1. Chemical structures of the Ru(II) photocatalysts **Ru1**−**Ru3**.

In metal-based photocatalytic cancer drug development, NADH is one of the target molecules for in-cell catalysis, as it has been discovered that the NADH coenzyme level in cancer cells is higher than that of normal cells.[23−27] NADH is also very crucial for many intracellular biochemical processes such as (i) functions of ca. 400 oxidoreductases, (ii) ATP generation, (iii) maintenance of in-cell redox balance and cellular metabolism, (iv) main electron donor in the mitochondrial electron transfer chain, etc.[26−29] Thus, systematic oxidation of NADH to NAD^+ in cancer cells using a low nontoxic catalytic amount of the drug can present an alternative cancer cell death mechanism.[8,14] In metal-based photocatalytic cancer drug development research, Ir(III) photocatalysts dominated mostly due to their excited state photochemistry.[30−32] In 2019, for the first time, Sadler and co-workers achieved blue light-triggered in-cell NADH oxidation with an Ir(III) photocatalyst, which induced immunogenic apoptosis in cancer cells by altering the intracellular NAD^+/NADH ratio.[21] Subsequently, our group and Huang's group have reported several other highly efficient green light-active Ir(III)-based photocatalysts for photocatalytic cancer drug development.[10−12] Recently, Deng *et al.* achieved NIR light-triggered anticancer activity in hypoxic tumors with the carbo/oxaliplatin derivative of Pt(IV) prodrug by oxidizing NADH.[33]

On the other hand, Ru(II)-based photosensitizers with attractive photostability, excited state chemistry, and tunable photophysics/photochemistry are widely used in cancer photodynamic therapy (PDT) research.[34−47] Ru(II)-based TLD1433 from McFarland's group obtained fast-track approval from the FDA as a green light PDT agent for bladder cancer.[39] Chao *et al.* developed Ru(II)-based PDT agents with biotin as the tumor-targeting group.[48] The complexes showed excellent phototoxicity (IC_{50}, ca. 3.3 μM) toward the cisplatin-resistant A549R cancer cells upon irradiation of two-photon light (800 nm, 0.27 mW cm^{-2}, 80 MHz, 100 fs).[48] Turro and co-workers showed photoinduced phosphine ($-PPh_3$) exchange from Ru(II) polypyridyl complexes on visible light irradiation, and these complexes showed >4−6 toxicity against the MDA-MB-231 cells upon blue light irradiation than dark.[49] Bonnet *et al.* developed a tris-heteroleptic Ru(II) prodrug with 2-methylthiomethylpyridine (mtmp).[50] This complex cleaved off mtmp after green light irradiation (520 nm, 19 J/cm^2) and bound to DNA to promote apoptosis.[50] Interestingly, the complex did not inhibit the growth of tumors in the ectopic tumor models but significantly inhibited the growth of tumors in orthotopic tumor models.[50] Recently, Glazer's group developed red light-responsive Ru(II)-based photocages with a CYP1B1 (cancer-associated cytochrome P450 enzyme) inhibitor.[51] These prodrugs released cytochrome inhibitors upon exposure to red light (600 nm, 58.7 J/cm^2).[51] These inhibitors inhibited CYP1B1 with an IC_{50} of 300 pM.[51] Gasser's group reported several important Ru(II) polypyridyl complexes as efficient PDT agents.[52−54]

Significantly, Ru(II) complexes are being widely used for PDT application, but the potential of Ru(II) complexes in in-cell catalysis is not fully realized, such as in the oxidation of NADH. Recently, our group and Huang's group showed the usefulness of Ru(II) photocatalysts (only 3 reports so far) for developing green and red light photocatalytic anticancer drugs.[13,14] We reported green/red light-responsive Ru(II) complexes, viz., $[Ru(bpy)_2(bpy\text{-}dph)]Cl_2$ and $[Ru(bnp)(tpy\text{-}pyren)](PF_6)_2$ (bpy = 2,2′-bipyridine, bpy-dph = 4,4′-diphenyl-2,2′-bipyridine, bnp = 2,6-bis(2-naphthyridyl)-pyridine, and tpy-pyren = 4′-(pyren-1-yl)-2,2′:6′,2″-terpyridine), which induced apoptotic cancer cell death through NAD(P)H oxidation and diverse ROS generation via synergistic type I and type II pathways.[13,14] Interestingly, $[Ru(bnp)(tpy\text{-}pyren)](PF_6)_2$ was found to overcome drug resistance via intracellular glycerophospholipid, lipid, and peptide metabolism inhibition as a result of NAD(P)H photo-oxidation.[14] As only three reports are available with Ru(II) photocatalysts in photocatalytic cancer drug development research, more investigations with Ru(II) photocatalysts are needed to decide the fate of photoresponsive Ru(II) complexes in photocatalytic cancer therapy. Thus, in this work, we have developed two green light-responsive Ru(II) complexes, viz., $[Ru(ph\text{-}tpy)(phen)Cl]PF_6$ (**Ru2**), $[Ru(ph\text{-}tpy)(aip)Cl]PF_6$ (**Ru3**) (Figure 1), as efficient NADH photo-oxidation catalysts. The complex $[Ru(ph\text{-}tpy)(bpy)Cl]PF_6$ (**Ru1**) was used as a control. The detailed anticancer investigation with **Ru2** and **Ru3** revealed that these complexes are remarkably phototoxic in green and visible light, which was also supported by the DFT calculation data. The anticancer activities of these complexes originated from their intracellular production of ROS and photo-oxidation of NADH.

https://doi.org/10.1021/acs.inorgchem.4c00650
Inorg. Chem. 2024, 63, 7493−7503

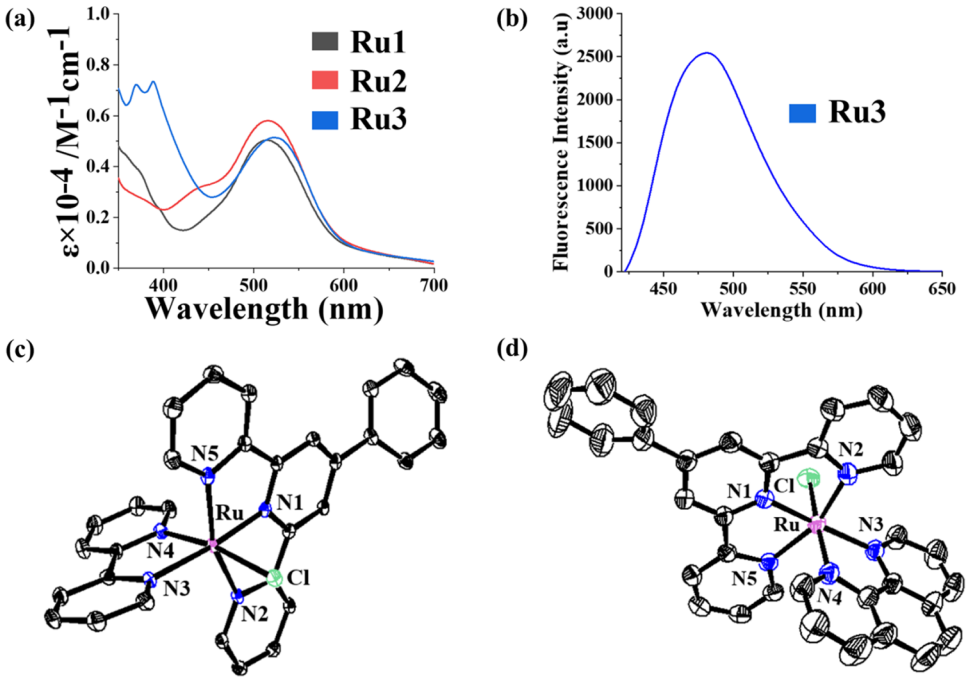

Figure 2. (a) Absorption spectra of complexes (**Ru1**−**Ru3**) in DMSO. (b) Emission spectrum of **Ru3** in DMSO (λ_{ex}: 425 nm). ORTEP diagram of the cationic complex of (c) **Ru1** and (d) **Ru2** with thermal ellipsoids at a 50% probability level, along with the atom numbering of the heteroatoms in $[RuN_5Cl]PF_6$. The counter-anion (PF_6) and hydrogens are omitted for clarity.

RESULTS AND DISCUSSION

Synthesis and Characterization. Ru(II) complexes (**Ru1**−**Ru3**) were synthesized by reacting 1 equiv. of $RuCl_3 \cdot xH_2O$ with 1.0 equiv. of phenyl-terpyridine followed by the addition of 1.0 equiv. of bpy (**Ru1**)/phen (**Ru2**)/aip (**Ru3**) in ethanol. The complexes were isolated as PF_6^- salt after adding excess NH_4PF_6 (Figure S1). All three Ru(II)-based complexes were characterized by elemental analysis, HRMS, ^{1}H NMR, UV−vis and fluorescence spectroscopy, FT-IR, and SC-XRD (for complexes **Ru1** and **Ru2**) (Figures S2−S12). The most abundant peak in HRMS corresponded to $[M]^+$ in acetonitrile, confirming the formation of **Ru1**−**Ru3**. In the ^{1}H NMR of complexes **Ru1**−**Ru3**, the characteristic peaks were obtained in the aromatic region. Interestingly, the N−H peak of the imidazole ring of aip (δ = 14.20 ppm) disappeared upon coordinating with the Ru(II) center, in line with previous studies.[55,56] An intense metal-to-ligand charge transfer (MLCT) band of **Ru1**−**Ru3** was observed at ca. 440−600 nm in DMSO (Figure 2a).[57−59] **Ru3** showed an additional peak near 380 nm corresponding to aip (anthracene)-based $\pi-\pi^*$ transition.[55] The absorption of green light might be useful for achieving green light-activated cancer therapy via in-cell NADH oxidation.[10,13] In DMSO solution, **Ru3** showed an emission band near ca. 500 nm upon 425 nm excitation due to the presence of the anthracene moiety (Figure 2b).

X-ray Crystallography. The structures of **Ru1** and **Ru2** were determined by SC-XRD. Slow evaporation of an acetonitrile−toluene (1:1 (v/v)) solution of the complexes produced reddish-brown crystals for diffraction. Both complexes (**Ru1** and **Ru2**) crystallized in a monoclinic system with the $P12_1/c$ space group (Table S1). The ORTEP view of the complexes is given in Figure 2c,d. The unit cell packing diagram of **Ru1** and **Ru2** is given in Figure S13. The crystal structures of **Ru1** and **Ru2** revealed their distorted octahedral geometry, in which the Ru center was surrounded by five N and one Cl. Four molecules are present in the one-unit cell of both **Ru1** and **Ru2** (Figure S13 in the Supporting Information). The obtained crystal structures of **Ru1** and **Ru2** were similar to previously reported Ru(II) complexes with the same coordination sphere.[60,61] The selected bond distances and bond angles are listed in Table 1. The Ru−Cl bonds (2.4008 Å for **Ru1** and 2.4078 Å for **Ru2**) were the longest among all of the coordinating bonds, indicating their presence at the axial position. However, the observed Ru−Cl bond

Table 1. Selected Bond Distances (Å) and Bond Angles (deg) of Complexes Ru1 and Ru2

	Ru1	Ru2
Ru−Cl	2.4008 (7)	2.4078 (8)
Ru−N1	1.954 (2)	1.950 (2)
Ru−N2	2.069 (2)	2.064 (2)
Ru−N3	2.083 (2)	2.092 (2)
Ru−N4	2.036 (2)	2.042 (2)
Ru−N5	2.066 (2)	2.065 (2)
Cl−Ru−N1	89.07 (6)	92.02 (7)
Cl−Ru−N2	91.17 (6)	92.53 (7)
Cl−Ru−N3	94.99 (6)	92.85 (7)
Cl−Ru−N4	170.48 (6)	170.97 (7)
Cl−Ru−N5	88.47 (6)	87.90 (7)
N1−Ru−N2	79.75 (9)	80.0 (1)
N1−Ru−N3	174.65 (9)	173.5 (1)
N1−Ru−N4	98.01 (9)	95.8 (1)
N1−Ru−N5	79.43 (9)	79.20 (9)
N2−Ru−N3	96.64 (8)	95.5 (1)
N2−Ru−N4	96.33 (9)	93.2 (1)
N2−Ru−N5	159.19 (8)	159.1 (1)
N3−Ru−N4	78.37 (8)	79.7 (1)
N3−Ru−N5	104.12 (8)	105.3 (9)
N4−Ru−N5	86.59 (8)	89.2 (1)

https://doi.org/10.1021/acs.inorgchem.4c00650
Inorg. Chem. 2024, 63, 7493−7503

lengths were slightly less than the previously reported complexes with similar structures.[60,61] The shortest bond length between Ru and the central nitrogen atom of the terpyridine ligand (Ru−N1) in both complexes **Ru1** (1.954 Å) and **Ru2** (1.950 Å) is comparable to the previously reported complexes.[60,61] Interestingly, in both complexes, the bond length Ru−N4, i.e., trans to Cl^-, is relatively shorter than those of other Ru−N bonds (Table 1). The trans bond angles Cl−Ru−N4 and N1−Ru−N3 in **Ru1** and **Ru2** are about 10° distorted from the ideal angle. For the N2−Ru−N5 angle, the highest distortion of around 21° was found (159.19° and 159.1° for **Ru1** and **Ru2**, respectively), in line with previous studies.[60,61]

Solubility, Stability, and Lipophilicity. The solubility of the complexes (**Ru1**−**Ru3**) was measured in different solvents. Complexes were soluble in nonchlorinated polar solvents like acetone, DMF, DMSO, and acetonitrile and partially soluble in methanol, ethanol, and H_2O. The photostability of the complexes (**Ru1**−**Ru3**) was monitored via time-dependent UV−vis studies under white light. **Ru1**−**Ru3** in PBS-DMSO (99:1 v/v) showed no marked changes in spectra and absorbance (Figure S14), revealing that these complexes might be used as stable photocatalysts. To assess the lipophilicities of the complexes, their partition coefficients (log $P_{o/w}$) were determined in octanol and water. The log $P_{o/w}$ parameter reflects the distribution of the complex between water and octanol, providing insights into the potential cellular uptake through passive diffusion.[62−64] A positive log $P_{o/w}$ value indicates a preference for the octanol layer, while a negative value suggests a preference for water.[62−65] The log $P_{o/w}$ values for the complexes **Ru1**, **Ru2**, and **Ru3** were 1.25, 1.47, and 2.31, respectively (Figure S15). The log $P_{o/w}$ values increased from **Ru1** to **Ru3**, aligning with the enlargement of the lipophilic moiety in the bidentate *N,N*-ligand. Considering the established correlation between cellular uptake, lipophilicity, and cytotoxicity,[65,66] it is plausible to anticipate that **Ru3** could show the highest cellular uptake and phototoxicity within the series.

DFT Calculation. The DFT calculations were performed for **Ru1**−**Ru3** to understand their electronic structure and photophysical properties. To optimize the structure, the ωB97X-D function was applied with the def2-SVP basis set for all atoms in water using the CPCM implicit solvation model.[67] The optimized structures of **Ru1**−**Ru3** indicated that the Ru(II) center is coordinated with *N,N,N*-donor and *N,N*-donor ligands and one Cl atom in a distorted octahedral manner with a $Ru^{II}N_5Cl$ coordination core, similar to the crystal structure of the complexes (Figure 3). The frontier molecular orbitals (FMOs) of **Ru1**−**Ru3** revealed that the highest occupied molecular orbital (HOMO) is distributed partially on the Ru center and, to some extent, the *N,N*-donor moiety (Figure S16). The lowest unoccupied molecular orbital (LUMO) resides on the *N,N,N*-donor phenyl terpyridine moiety for all complexes. Further, we have calculated the absorption and emission energies at the TD-ωB97X-D/def2TZVP level of theory in water. The lowest $S_0 \rightarrow S_1$ transition energy is ∼2.5 eV (Table S2) for these complexes, and natural transition orbital (NTO) plots (Figure 3) show ^{1}MLCT from Ru to the *N,N,N*-donor ligand. Next, we have optimized the triplet states of these complexes using the UωB97X-D/def2-SVP level of theory and determined the singlet−triplet energy gap ($\Delta E_{S\text{-}T}$), spin density plots, and SOMO plots at the UωB97X-D/def2-SVP level of theory. For

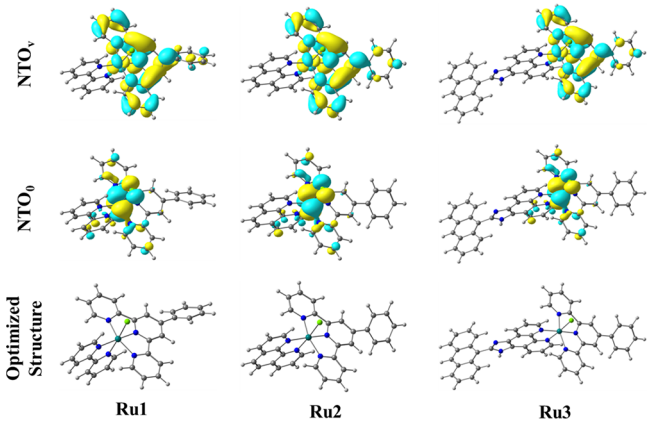

Figure 3. Top, center, and bottom of each image, respectively, display the virtual natural transition orbital (NTO$_v$), occupied natural transition orbital (NTO$_o$) for $S_0 \rightarrow S_1$ transition, and optimized structures of **Ru1**−**Ru3**.

Ru1 and **Ru2**, SOMO and SOMO-1 are predominantly localized on the metal center and the *N,N,N*-donor ligand, whereas for **Ru3**, SOMO is located on Ru and *N,N,N*-donor ligand and SOMO-1 on anthracene (Figure S17). The spin density plots also reveal that spin is localized on Ru and the *N,N,N*-donor ligand (Figure S18). The calculated lowest triplet energies for **Ru1**, **Ru2**, and **Ru3** are 2.23, 1.91, and 1.96 eV respectively, which are higher than that for $^3O_2$ (0.98 eV), suggesting that these complexes can generate singlet oxygen (Table S3).

Green Light-Induced Photocatalytic Oxidation of NADH. NADH, a crucial molecule for cellular redox balance maintenance, serves as an electron carrier and coenzyme in several metabolic pathways.[23−27] Its pivotal involvement in electron transfer, energy production, and enzyme regulation makes it necessary for the normal functioning of cells and overall cellular health.[23−27] Any unnatural alteration in the intracellular NADH concentration can disrupt the mitochondrial ETC, intracellular redox harmony, and energy production, ultimately leading to cell death.[23−27] This concept has been used by Sadler and co-workers to achieve light-triggered anticancer activity with an Ir(III) complex.[21] Further, Huang's group and our group generalized this concept with both Ir(III) and Ru(II) complexes to produce synergistic oxygen-based ROS generation and NADH oxidation to obtain light-triggered anticancer effects against different cancer cell lines.[10−14] Henceforth, the NADH photo-oxidation ability of **Ru1**−**Ru3** was investigated using UV−vis spectroscopy by monitoring the intensity of the NADH characteristic band at 339 nm and the NAD^+ characteristic band at 259 nm in a PBS-DMSO (99:1 v/v) solution.[13,14,68] **Ru1**−**Ru3** (10 μM) did not show any changes in the absorption spectra of NADH (240 μM) in the dark (Figure S19b−d in the Supporting Information). Upon green light (525 nm, 50.2 J cm^{-2}) irradiation, **Ru2** and **Ru3** decreased the characteristic absorbance of NADH significantly and simultaneously increased the absorbance of the NAD^+ characteristic band (Figure 4a,b). **Ru1** on green light exposure caused NADH oxidation but with low turnover frequency (TOF) (ca. 10.9 h^{-1}) (Figure S19a in the Supporting Information). This result indicated the photo-oxidation of NADH by **Ru2** and **Ru3** upon green light exposure. **Ru2** oxidized NADH with a turnover frequency (TOF) of ca. 55.5 h^{-1}. The TOF of **Ru3** was ca. 118.2 h^{-1}, the most potent

https://doi.org/10.1021/acs.inorgchem.4c00650
Inorg. Chem. 2024, 63, 7493−7503

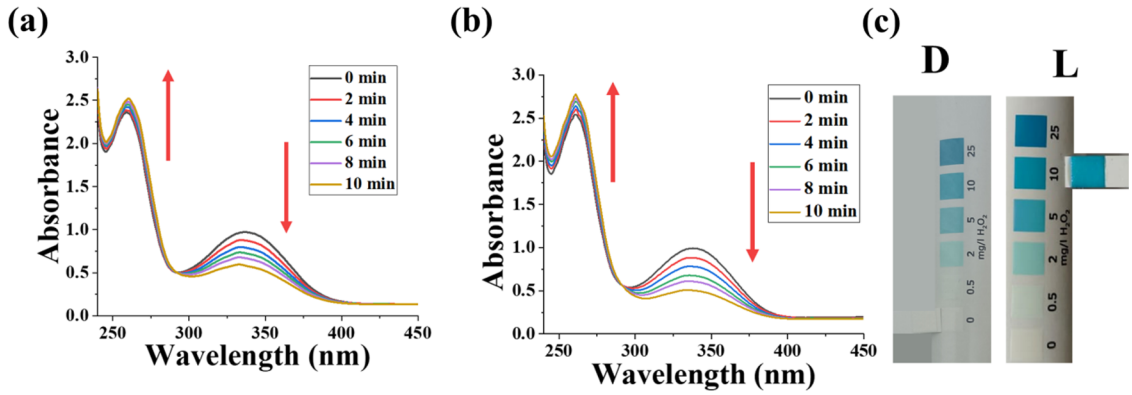

Figure 4. Photocatalytic oxidation of NADH (240 μM) by **Ru2** (10 μM) (a) and **Ru3** (6 μM) (b) in a PBS-DMSO (99:1 v/v) (pH = 7.4) solution (light source: 525 nm, 50.2 J cm^{-2}). (c) Detection of H_2O_2 generation by **Ru3** (6 μM) during NADH (240 μM) oxidation under dark (D) and light irradiation (L) in a DMSO-PBS (99:1 v/v) solution (light source: 525 nm, 50.2 J cm^{-2}).

NADH photocatalyst among these complexes. The better NADH photo-oxidation ability of **Ru3** might be due to its low ΔE_g value. Importantly, **Ru3** was a better photocatalyst than the first reported Ir(III)-based NADH oxidation photocatalyst.[21] **Ru3** also showed equivalent or better NADH oxidation TOF than other reported Ru(II)/Ir(III)-based photocatalysts (Table S4). Overall, the observed excellent NADH photo-oxidation ability of **Ru3** might contribute to its phototoxicity via in-cell NADH oxidation.[13,14] Furthermore, upon green light irradiation (light source: 525 nm, 50.2 J cm^{-2}), **Ru3** generates H_2O_2 in the presence of NADH (Figure 4c). This indicates that molecular O_2 is involved in the catalytic process, like the Ir(III) photocatalysts reported in the literature.[10−12,21] O_2 is probably involved in the regeneration of the Ru(II) active catalyst.[13−15]

Cellular Uptake. The adequate internalization of any drug candidate is a crucial factor for high therapeutic value.[69−71] High in-cell uptake of cancer therapeutic agents is reported to enhance their anticancer potential.[69−71] Uptake studies were conducted by quantifying the cellular ruthenium content using inductively coupled plasma mass spectrometry (ICP-MS) in HeLa cells (Figure S20 in the Supporting Information). Following 6 h of incubation with the **Ru1**−**Ru3** complexes (10 μM) in the dark, the cells were lysed and processed in a 2% HNO_3 solution. Table 2 reveals that **Ru3** exhibited the highest

Table 2. Intracellular Ru Content for Ru1−Ru3 after 6 h of Incubation with HeLa Cells

complex	Ru content in whole cell lysate (ng/10^6 cells)
Ru1	52.4 ± 2.2
Ru2	58.7 ± 3.1
Ru3	80.2 ± 4.7

internalization, with a Ru content of 80.2 ± 4.7 ng/10^6 cells, followed by **Ru2** (58.7 ± 3.1 ng/10^6 cells) and **Ru1** (52.4 ± 2.2 ng/10^6 cells). These results align with the log $P_{o/w}$ values of the complexes. The highest intracellular uptake of **Ru3** is certainly due to its higher lipophilicity.[62,72,73] Thus, **Ru3** might act as a much better photocytotoxic agent.

Cytotoxicity Studies. The sufficient cellular uptake of **Ru1**−**Ru3** encouraged us to evaluate their cytotoxicity against the HeLa cancer cell line and normal splenocyte in both the dark and white/green light by MTT assay.[69] **Ru1**−**Ru3** showed no notable dark toxicity toward the normal cells (IC_{50} > 50 μM) (Table 3 and Figure S21). In the dark, **Ru1**−**Ru3** did not show any significant cytotoxicity (IC_{50} > 60 μM) toward HeLa cells (Table 3 and Figure S22). However, upon white light (400−700 nm, 5.0 J cm^{-2}) exposure, the cytotoxicity of **Ru1**−**Ru3** was enhanced significantly (Table 3 and Figure S23). Among the complexes, **Ru3** (IC_{50} = 0.75 ± 0.12 μM) showed better activity as compared to **Ru1** (IC_{50} = 6.84 ± 0.21 μM) and **Ru2** (IC_{50} > 10 μM) against HeLa cells. A similar trend of photocytotoxicity was observed under green light (IC_{50}: **Ru3** = 1.9 ± 0.2 μM; **Ru1** = 8.4 ± 5.0 μM; **Ru2** ≥ 10 μM) (Figure S24). The high anticancer effect of **Ru3** might be due to its higher cellular uptake and the presence of photoresponsive aip ligand with much higher π-conjugation. Previous reports have shown that the presence of an imidazole ring in aip causes cell cycle arrest and subsequently induces apoptosis against cancer cells.[74,75] Also, Chao *et al.* reported the dark toxicity of [Ru(ph-tpy)(bpy)Cl]ClO_4 on 48 h of incubation against HeLa cells.[76] It showed an IC_{50} of *ca.* 51.4 μM under those conditions.[76] With respect to our previous work, **Ru3** showed better activity than [Ru(bpy)$_2$(bpy-dph)]Cl_2 (IC_{50} = 0.3 μM).[13] **Ru3** showed similar or better anticancer responses than some of the previously reported Ru(II)-based phototherapeutic agents with similar structures in HeLa cells (Table 2).[10,46,77−80] For example, [Ru(bpy)(dppn)-(phpy)]PF_6 gave an IC_{50} value of 7 μM in HeLa cells, but in the dark.[77] [Ru(dppz-X_2)$_3$]$(PF_6)_2$ (X = H and F) showed no toxicity in the dark, but upon light irradiation (light source: 9.27 J cm^{-2}), it showed IC_{50} values of ca. 2 and 5.5 μM, respectively.[78] [Ru(bipy)$_2$dppz-7-acetoxy]$(PF_6)_2$ showed no dark toxicity (>100 μM) but showed IC_{50} of ca. 9.0 and 5.5 μM on changing light dose from 2.58 to 9.27 J cm^{-2}, respectively.[46] [Ru(dqpCO_2Me)(ptpy)]$(PF_6)_2$ showed no dark toxicity (>100 μM) toward HeLa cells even after 48 h of incubation, but on treatment of light (6.95 J cm^{-2}), it showed moderate toxicity (IC_{50} = 25.3 ± 4.7 μM).).[79] Besides that, IC_{50} values of **Ru1**−**Ru3** are much better than those of the clinically used photosensitizer 5-ALA (151.1 μM) and cisplatin (25.3 μM) upon green light irradiation (29.56 J cm^{-2}). The choice of light in PACT plays a vital role in achieving anticancer activity.[10]

ROS Generation. ROS are naturally formed as byproducts of cellular metabolism in various physiological processes in the human body.[80,81] However, increased ROS levels can cause oxidative stress or inflammation and damage cells and cellular components.[80] Therefore, in photoactivated cancer therapy,

https://doi.org/10.1021/acs.inorgchem.4c00650
Inorg. Chem. 2024, 63, 7493−7503

Table 3. IC_{50} (μM) Values of Ru1−Ru3 and Some Ru(II)-Based Complexes against HeLa Cells in the Dark and upon Light Irradiation

	HeLa							splenocytes
		light (wavelength) (nm)						
complex	dark	400−700	525	350	420	PI (400−700 nm)	PI (525 nm)	dark
Ru1[a]	94.2 ± 2.8	6.8 ± 0.2	8.5 ± 5.0			13.77	11.11	55.6 ± 1.3
Ru2[a]	95.5 ± 2	>10	>10			NA	NA	79 ± 3
Ru3[a]	66.2 ± 2	0.75 ± 0.12	1.9 ± 0.2			88.37	34.52	75.7 ± 2.2
[Ru(ph-tpy)(bpy)Cl]ClO_4[b]	51.4							
[Ru(bpy)$_2$(bpy-dph)]Cl_2[c]	140.7		0.3				469	
[Ru(bpy)(dppn)(phpy)]PF_6[d]	7							
[Ru(dppz-H_2)$_3$]$(PF_6)_2$[e]	>100				2			
[Ru(dppz-F_2)$_3$]$(PF_6)_2$[e]	>100				5.5			
[Ru(bipy)2dppz-7-acetoxy]$(PF_6)_2$[f]	>100			9	5.5			
[Ru(dqpCO_2Me)(ptpy)]$(PF_6)_2$[g]	>100				25.3 ± 4.7			
cisplatin[h]	16.5		25.3					
5-ALA[h]	>10000		151.1				6.6	

[a]White light irradiation; light treatment: incubation time of 6 h, total irradiation = 5.0 J cm^{-2} over 30 min. Recovery time of 18 h. Green light irradiation; light treatment: incubation time of 6 h, total irradiation = 50.2 J cm^{-2} over 30 min. Recovery time of 18 h. Dark treatment: incubation time of 6 h, recovery time of 18 h. [b]Dark treatment: incubation time of 48 h (from ref 76). [c]Green light irradiation (525 nm, 29.56 J cm^{-2}). Light treatment: incubation time of 8 h, total irradiation = 29.56 J cm^{-2}. Recovery time of 40 h. Dark treatment: incubation time of 8 h, recovery time of 40 h (from ref 13). [d]Dark treatment: incubation time of 2 h, recovery time of 24 h (from ref 77). [e]Dark treatment: incubation time of 48 h, light irradiation (420 nm, 9.27 J cm^{-2}). Light treatment: incubation time of 4 h, total irradiation = 9.26 J cm^{-2} over 20 min. Recovery time of 44 h (from ref 78). [f]Dark treatment: incubation time of 48 h, light irradiation (350 nm, 2.58 J cm^{-2}). Light treatment: incubation time of 4 h, total irradiation = 2.58 J cm^{-2} over 10 min. Recovery time of 44 h. Light irradiation (420 nm, 9.27 J cm^{-2}). Light treatment: incubation time of 4 h, total irradiation = 9.27 J cm^{-2} over 20 min. Recovery time of 44 h (from ref 46). [g]Light irradiation (420 nm, 6.95 J cm^{-2}). Light treatment: incubation time of 4 h, total irradiation = 6.95 J cm^{-2} over 30 min. Recovery time of 44 h. Dark treatment: incubation time of 4, 48 h, recovery time of 44 h (from ref 79). [h]Green light irradiation (525 nm, 29.56 J cm^{-2}). Light treatment: incubation time of 8 h, light irradiation = 29.56 J cm^{-2}. Recovery time of 40 h. Dark treatment: incubation time of 8 h, recovery time of 40 h (from ref 10).

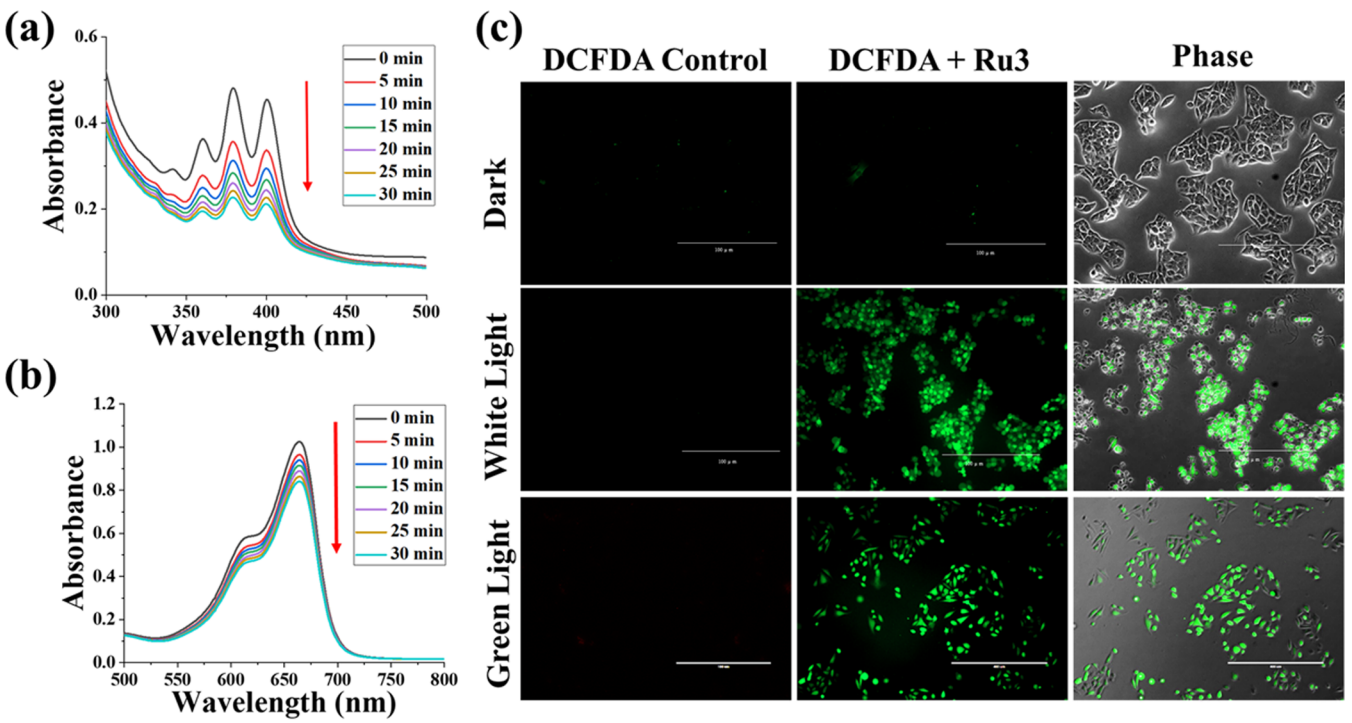

Figure 5. (a) Time-dependent decrease in the absorbance of DPA, indicating $^1O_2$ generation by **Ru3** (10 μM) in a PBS-DMSO (99:1 v/v) solution upon green light irradiation. (b) Time-dependent degradation of MB, indicating $OH^{\bullet}$ generation by **Ru3** (10 μM) in a PBS-DMSO (99:1 v/v) solution on green light irradiation (light source: 525 nm, 50.2 J cm^{-2}). (c) In-cell ROS generation by **Ru3** + dark, **Ru3** + white light (400−700 nm, 5.0 J cm^{-2}), and **Ru3** + green light (light source: 525 nm, 50.2 J cm^{-2}) in HeLa cells after 30 min of incubation. Scale bar: 400 μm.

controlled ROS generation has been used to selectively destroy cancer cells while sparing healthy ones.[81] ROS are reported to damage cancer cells by primarily damaging their DNA, proteins, and cell membranes, ultimately triggering apoptosis or necrosis.[80−82] In photocatalytic cancer therapy, the photoresponsive metal complexes are reported to produce

https://doi.org/10.1021/acs.inorgchem.4c00650
Inorg. Chem. 2024, 63, 7493−7503

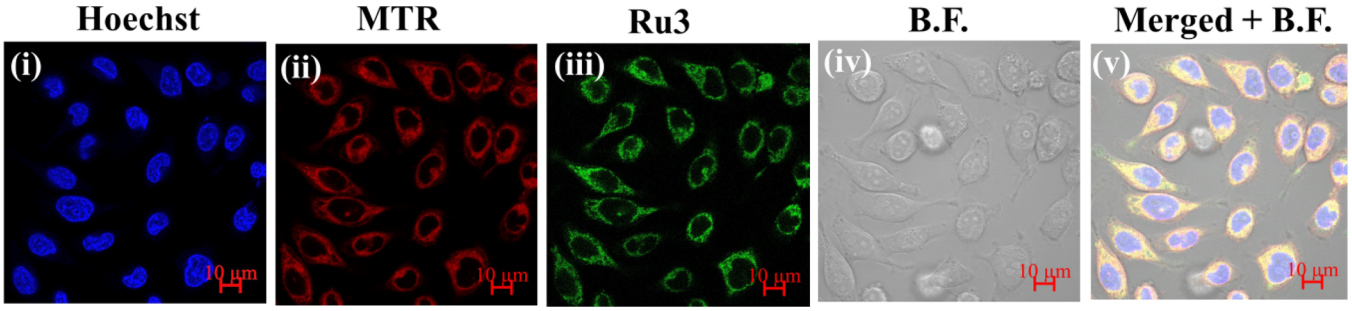

Figure 6. Confocal images of HeLa cells incubated with **Ru3** (15 μM), the nucleus-specific blue-emitting dye Hoechst, and MitoTracker Red (MTR). Panel (i) shows blue emission of nucleus staining dye Hoechst (λ_{ex} ~ 405 nm and λ_{em} ~ 460 nm), panel (ii) shows red emission of MTR (λ_{ex} ~ 630 nm and λ_{em} ~ 650 nm), panel (iii) shows green emission of **Ru3** (λ_{ex} ~ 488 nm and λ_{em} ~ 500 nm), panel (iv) shows a bright field image, and panel (v) shows a merged image. Scale bars, 10 μm.

H_2O_2, $OH^{\bullet}$, and $O_2^{\bullet-}$ (as the byproducts of NADH oxidation) in addition to $^1O_2$ (via a type II energy transfer pathway).[8−14] The encouraging photophysical properties, DFT calculation data, and enhanced light-triggered cytotoxicity indicated that **Ru1**−**Ru3** could have a notable ROS generation tendency. To examine the $^1O_2$ production efficiency of **Ru1**−**Ru3**, 9,10-diphenyl anthracene (DPA) has been used. In the dark, **Ru1**−**Ru3** (10 μM) did not cause any notable change in DPA-based absorbance, indicating inefficiency in $^1O_2$ generation without light. However, **Ru1**−**Ru3** efficiently generated $^1O_2$ upon green light exposure (Figure 5a and Figure S25a,b in the Supporting Information). **Ru3** emerged as a more potent $^1O_2$ generator than **Ru1** and **Ru2**, as demonstrated by a notable decrease in the DPA-based absorption bands. This observation indicates that the high photocytotoxicity of **Ru3** partially can be due to light-induced high amounts of $^1O_2$ generation. Furthermore, the $OH^{\bullet}$ generation tendency of **Ru1**−**Ru3** was determined with methylene blue (MB), an $OH^{\bullet}$ probe. A similar trend of activity was obtained for $OH^{\bullet}$ generation by **Ru1**−**Ru3** (Figure 5b and Figure S25c in the Supporting Information) in the presence of NADH. The $OH^{\bullet}$ generated due to the homolysis of H_2O_2 formed during the photooxidation of NADH (as discussed above). All of these data indicated that **Ru3** is an efficient type-I and type-II PS.

Furthermore, the in-cell ROS generation by **Ru3** was visualized by DCFDA assay in HeLa cells using fluorescence microscopy.[80−82] The nonfluorescent ROS marker 2′,7′-dichlorofluorescin diacetate (DCFH-DA) converts to highly green fluorescent 2′,7′-dichlorofluorescin (DCF) by the intracellular ROS.[80−82] As shown in Figure 5c, **Ru3** generated significant ROS at its IC_{50} concentrations only after light (white or green) exposure, being inactive under dark conditions, revealing that the remarkable phototoxicity of **Ru3** is also due to its highly efficient in-cell ROS generation (in addition to NADH oxidation). A similar ROS-mediated anticancer mechanism was also observed with the other Ru(II)-based photosensitizers like $[Ru(tpy)(N,N)(py)](PF_6)_2$ (where, *N*,*N* = 2,2′-bipyridine, 6,6′-dimethyl-2,2′-bipyridine, benzo[*i*]-dipyrido[3,2-a:2′,3′-c]phenazine, and 3,6-dimethyl-benzo [*i*]dipyrido [3,2-a:2′,3′-c]phenazine) and chiral $[Ru(Ph_2phen)_2(\kappa S,\kappa N\text{-(Ac-RGDH-NH}_2))]Cl_2$ (where Ph_2phen = 4,7-diphenyl-1,10-phenanthroline).[34−47,83,84]

Cellular Localization, Mitochondrial Dysfunction, and Cellular Apoptosis. The luminescence characteristics of the complexes serve as an important tool for monitoring their intracellular distribution.[13,47,66] The green emission from **Ru3** (on 488 nm laser excitation), in HeLa cells, affirms its potential for cellular imaging (Figure 6). The merged image, combining nuclear staining with Hoechst dye (blue fluorescent) and complex-based green emission, indicated cytosolic localization. Furthermore, the merged image with MitoTracker Red (MTR, red fluorescent) suggested the localization of **Ru3** in mitochondria, with a Pearson correlation coefficient (PCC) of 0.74 (Figure 6).

For the adenosine triphosphate (ATP) biosynthesis, required for cell survival and growth, mitochondria are essential.[85] Overload of ROS is reported to damage mitochondria via oxidative stress.[86] The alteration of mitochondrial membrane potential ($\Delta\Psi_m$) indicates mitochondrial dysfunction and damage.[86] As **Ru3** produced in-cell ROS on light activation, here, the alteration of $\Delta\Psi_m$ was visualized by JC-1 assay using fluorescence microscopy.[86] JC-1 dye produces red fluorescence when internalized within the mitochondria at high membrane potential ($\Delta\Psi$m), whereas at low membrane potential, JC-1 becomes green fluorescent.[87] As shown in Figure 7, in the dark, **Ru3** could not change the

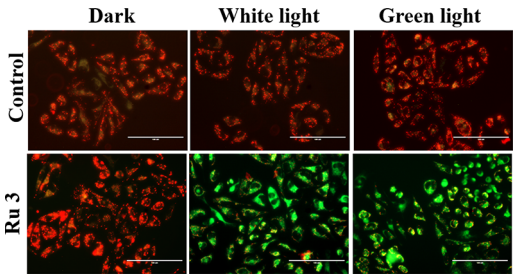

Figure 7. Visualization of the mitochondrial membrane potential change by **Ru3** + light via the JC-1 assay. Incubation of **Ru3** with HeLa cells for 4 h at IC_{50} concentration was followed by 20 min white light (400−700 nm, 5.0 J cm^{-2}) or green light (525 nm, 50.2 J cm^{-2}) irradiation. Scale bars, 100 μm.

$\Delta\Psi_m$, as indicated by the red fluorescence from JC-1, the same as the control. In contrast, in the cells with **Ru3** + light treatment, J-monomer-based green fluorescence was observed (Figure 7), indicating a change in $\Delta\Psi_m$. Overall, the above results indicate that **Ru3** selectively changes the $\Delta\Psi_m$ only after light activation. This change in $\Delta\Psi_m$ could be a signature of cellular apoptosis through mitochondrial pathways.[85−87]

The excellent light-activated cytotoxic effects of **Ru3** and the change in $\Delta\Psi_m$ by **Ru3** + light pushed us to study the underlying cell death mechanism induced by **Ru3** in the presence of light in HeLa cells. The changes in nuclear

https://doi.org/10.1021/acs.inorgchem.4c00650
Inorg. Chem. 2024, 63, 7493−7503

morphology were examined using Hoechst/PI dual staining at the IC_{50} concentration of **Ru3** to determine the mode of cell death. Nuclei of both live and apoptotic cells can be stained with Hoechst 33342 dye. When Hoechst 33342 binds to the nuclei of living cells, it is reported to emit a light blue fluorescence, whereas on binding to the apoptotic cells' nuclei, it is known to produce bright blue fluorescence. PI can only stain the nuclei of cells with compromised nuclear membranes and emits red fluorescence.[85−87] The result shown in Figure S26 revealed that **Ru3** did not show any cell death in the dark condition but produced apoptotic cell death responses (evident from round stressed cells, loss of cellular networks, bright condensed nuclei, and staining of the nuclei by PI) in the presence of both green light and white light (Figure 8 and

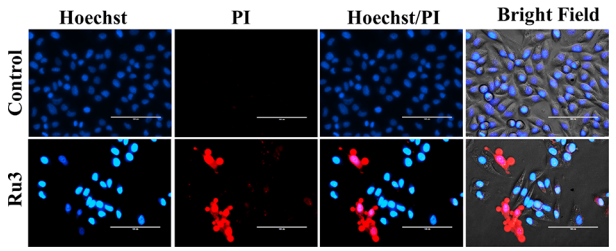

Figure 8. Green light-triggered apoptosis of HeLa cells induced by **Ru3** (750 nM) costained with Hoechst and PI. Scale bars, 100 μm.

Figure S27). Henceforth, from the above observations, it can be concluded that **Ru3** + light treatment promotes apoptosis in HeLa cells via ROS production and NADH photo-oxidation through a change in the $\Delta\Psi_m$.

CONCLUSIONS

In this work, we have synthesized, characterized, and evaluated the visible and green light-activated detailed anticancer activities of three terpyridine-based Ru(II) photocatalysts (**Ru1**−**Ru3**). The distorted octahedral geometry with a RuN_5Cl core of the complexes was evident from the single-crystal structures of complexes **Ru1** and **Ru2**. The photostable complexes showed an MLCT band at ca. 440−600 nm, which was very useful for the green-light NADH oxidation photocatalytic and photosensitizing activities (for ROS generation) of the complexes in an aqueous solution. **Ru2** and **Ru3** worked as efficient photocatalysts for NADH oxidation in an aqueous medium under green light exposure. The TOF of **Ru3** was much higher than $[Ir(ttpy)(pq)Cl]PF_6$.[21] Moreover, the efficiency of **Ru3** for the photocatalytic NADH oxidation was in the range of the most potent Ru(II)-based catalysts reported so far.[13−15] In the process of catalysis, molecular O_2 was converted to H_2O_2 via a type-I pathway. **Ru2** and **Ru3** also behaved as good green light photosensitizers to produce $^1O_2$ via the type-II pathway. **Ru3** also showed a higher intracellular uptake than **Ru1** and **Ru2**. The efficient intracellular uptake, good NADH oxidation, and ROS generation power of **Ru3** within mitochondria made it an excellent green light anticancer agent. **Ru1**−**Ru3** did not show any significant toxic effect toward normal splenocytes and HeLa cancer cells under dark conditions but showed remarkable nanomolar apoptotic toxicity upon irradiation of visible light or green light. **Ru3** has good PI values of ca. 88 and 34, respectively, upon white light or green light irradiation, which clearly indicates its selective anticancer activity upon light exposure. The green light-activated apoptotic antitumor activity of **Ru3** was the outcome of the synergism between its NADH oxidation capacity and ROS generation ability. The apoptotic cell death was initially started from the depolarization of mitochondria upon light irradiation. Overall, this study is a timely contribution to the progress of photocatalytic cancer drug development research. Moreover, this study also indicates that Ru(II)-based photocatalysts have a future as multifunctional photocatalytic anticancer agents.

ASSOCIATED CONTENT

Supporting Information

The Supporting Information is available free of charge at https://pubs.acs.org/doi/10.1021/acs.inorgchem.4c00650.

Tables for crystallographic data, FMO energies, singlet−singlet transition energies, and adiabatic singlet−triplet splitting energies; figures for characterization data (^1H and ^{13}C NMR, FT-IR, and HRMS), unit cell packing, photostability, partition coefficients, FMOs, SOMOs, isosurfaces of the spin density at triplet, NADH oxidation, ICP-MS standard calibration, cell viability from MTT assay, $^1O_2$ and $OH^•$ generation, and confocal images for the cell death mechanism (PDF)

Accession Codes

CCDC 2300105 and 2300106 contain the supplementary crystallographic data for this paper. These data can be obtained free of charge via www.ccdc.cam.ac.uk/data_request/cif, or by emailing data_request@ccdc.cam.ac.uk, or by contacting The Cambridge Crystallographic Data Centre, 12 Union Road, Cambridge CB2 1EZ, UK; fax: +44 1223 336033.

AUTHOR INFORMATION

Corresponding Authors

Arpan Bera − *Department of Inorganic and Physical Chemistry, Indian Institute of Science, Bangalore 560012, India*; Email: arpanbera@iisc.ac.in

Biplob Koch − *Department of Zoology, Institute of Science, Banaras Hindu University, Varanasi, Uttar Pradesh 221005, India*; Email: biplob@bhu.ac.in

Samya Banerjee − *Department of Chemistry, Indian Institute of Technology (BHU), Varanasi, Uttar Pradesh 221005, India*; orcid.org/0000-0003-4393-4447; Email: samya.chy@itbhu.ac.in

Authors

Arif Ali Mandal − *Department of Chemistry, Indian Institute of Technology (BHU), Varanasi, Uttar Pradesh 221005, India*

Virendra Singh − *Department of Zoology, Institute of Science, Banaras Hindu University, Varanasi, Uttar Pradesh 221005, India*

Sukanta Saha − *Department of Chemistry, Indian Institute of Technology Bombay, Mumbai, Maharashtra 400076, India*

Silda Peters − *Departmentof Chemistry, SRM Institute of Science and Technology, Kattankulathur, Tamil Nadu 603203, India*

Tumpa Sadhukhan − *Departmentof Chemistry, SRM Institute of Science and Technology, Kattankulathur, Tamil Nadu 603203, India*; orcid.org/0000-0003-1995-7286

Rajesh Kushwaha − *Department of Chemistry, Indian Institute of Technology (BHU), Varanasi, Uttar Pradesh 221005, India*

https://doi.org/10.1021/acs.inorgchem.4c00650
Inorg. Chem. 2024, 63, 7493−7503

Ashish Kumar Yadav − *Department of Chemistry, Indian Institute of Technology (BHU), Varanasi, Uttar Pradesh 221005, India*

Apurba Mandal − *Department of Chemistry, Indian Institute of Technology (BHU), Varanasi, Uttar Pradesh 221005, India*

Aarti Upadhyay − *Department of Inorganic and Physical Chemistry, Indian Institute of Science, Bangalore 560012, India*

Arnab Dutta − *Department of Chemistry, Indian Institute of Technology Bombay, Mumbai, Maharashtra 400076, India;* orcid.org/0000-0002-9998-6329

Complete contact information is available at: https://pubs.acs.org/10.1021/acs.inorgchem.4c00650

Author Contributions

S.B. and A.A.M. designed the studies and formulated the concept and overall project. A.A.M., A.K.Y., and A.M. synthesized, characterized, and crystallized the complexes. A.A.M. did all the in-solution chemistry. R.K., S.P., and T.S. performed the DFT calculation. S.S. and A.D. performed the SC-XRD measurements. V.S., B.K., A.B., and A.U. performed all the biological studies. The manuscript was written through the contributions of all authors. All authors have approved for the final version of the manuscript.

Notes

The authors declare no competing financial interest.

■ ACKNOWLEDGMENTS

We thank SERB (SRG/2022/000030), the Government of India, for financial support. B.K. acknowledges Banaras Hindu University, India, for providing fund under the IoE scheme (file no. R/Dev/D/IoE/Incentive/2021-22/32449). A.A.M., R.K., A.M., and A.K.Y thank the Ministry of Education, the Government of India, for the Prime Minister's Research Fellowship. We sincerely thank Ashish Kumar Maurya for his support during this work.

■ REFERENCES

(1) Sung, H.; Ferlay, J.; Siegel, R. L.; Laversanne, M.; Soerjomataram, I.; Jemal, A.; Bray, F. Global Cancer Statistics 2020: GLOBOCAN Estimates of Incidence and Mortality Worldwide for 36 Cancers in 185 Countries. *CA Cancer J. Clin.* **2021**, *71*, 209−249.

(2) Liang, G.; Sadhukhan, T.; Banerjee, S.; Tang, D.; Zhang, H.; Cui, M.; Montesdeoca, N.; Karges, J.; Xiao, H. Reduction of Platinum(IV) Prodrug Hemoglobin Nanoparticles with Deeply Penetrating Ultrasound Radiation for Tumor-Targeted Therapeutically Enhanced Anticancer Therapy. *Angew. Chem., Int. Ed.* **2023**, *62*, No. e2023010.

(3) Zhao, X.; Liu, J.; Fan, J.; Chao, H.; Peng, X. Recent progress in photosensitizers for overcoming the challenges of photodynamic therapy: from molecular design to application. *Chem. Soc. Rev.* **2021**, *50*, 4185−4219.

(4) Panda, T. R.; Manikandan, M.; Vaidya, S. P.; Chhatar, S.; Sinha, S.; Mehrotra, M.; Chakraborty, S.; Gadre, S.; Duari, P.; Ray, P.; Patra, M. The Power of Kinetic Inertness in Improving Platinum Anticancer Therapy by Circumventing Resistance and Ameliorating Nephrotoxicity. *Angew. Chem., Int. Ed.* **2023**, *62*, No. e202303958.

(5) Vigueras, G.; Gasser, G. Anticancer platinum-based photooxidants in a new light. *Nat. Chem.* **2023**, *15*, 896−898.

(6) Rottenberg, S.; Disler, C.; Perego, P. The rediscovery of platinum-based cancer therapy. *Nat. Rev. Cancer* **2021**, *21*, 37−50.

(7) Wang, X.; Wang, X.; Jin, S.; Muhammad, N.; Guo, Z. Stimuli-Responsive Therapeutic Metallodrugs. *Chem. Rev.* **2019**, *119*, 1138−1192.

(8) Liu, Z.; Sadler, P. J. Organoiridium Complexes: Anticancer Agents and Catalysts. *Acc. Chem. Res.* **2014**, *47*, 1174−1185.

(9) Zhu, Z.; Wei, L.; Yadav, A. K.; Fan, Z.; Kumar, A.; Miao, M.; Banerjee, S.; Huang, H. Cyanine-Functionalized 2,2′-Bipyridine Compounds for Photocatalytic Cancer Therapy. *J. Org. Chem.* **2023**, *88*, 626−631.

(10) Fan, Z.; Rong, Y.; Sadhukhan, T.; Liang, S.; Li, W.; Yuan, Z.; Zhu, Z.; Guo, S.; Ji, S.; Wang, J.; Kushwaha, R.; Banerjee, S.; Raghavachari, K.; Huang, H. Single-Cell Quantification of a Highly Biocompatible Dinuclear Iridium(III) Complex for Photocatalytic Cancer Therapy. *Angew. Chem., Int. Ed.* **2022**, *134*, No. e202202098.

(11) Zhu, Z.; Wei, L.; Lai, Y.; Carter, O. W. L.; Banerjee, S.; Sadler, P. J.; Huang, H. Photocatalytic glucose-appended bio-compatible Ir(III) anticancer complexes. *Dalton Trans.* **2022**, *51*, 10875−10879.

(12) Wei, L.; Kushwaha, R.; Dao, A.; Fan, Z.; Banerjee, S.; Huang, H. Axisymmetric bis-tridentate Ir(III) photoredox catalysts for anticancer phototherapy under hypoxia. *Chem. Commun.* **2023**, *59*, 3083−3086.

(13) Fan, Z.; Xie, J.; Kushwaha, R.; Liang, S.; Li, W.; Mandal, A. A.; Wei, L.; Banerjee, S.; Huang, H. Anticancer Screening of Ru(II) Photoredox Catalysts at Single Cancer Cell Level. *Chem.—Asian J.* **2023**, *18*, No. e202300047.

(14) Wei, S.; Liang, H.; Dao, A.; Xie, Y.; Cao, F.; Ren, Q.; Yadav, A. K.; Kushwaha, R.; Mandal, A. A.; Banerjee, S.; Zhang, P.; Ji, S.; Huang, H. Perturbing tumor cell metabolism with a Ru(II) photoredox catalyst to reverse the multidrug resistance of lung cancer. *Sci. China Chem.* **2023**, *66*, 1482−1488.

(15) Dao, A.; Wu, H.; Wei, S.; Huang, H. Novel Ru(II) complexes with multiple anticancer photoreactivity: ligand exchange, photoredox catalysis, reactive oxygen generation and endoperoxide formation. *Phys. Chem. Chem. Phys.* **2023**, *25*, 20001−20008.

(16) Dharmaraja, A. T. Role of Reactive Oxygen Species (ROS) in Therapeutics and Drug Resistance in Cancer and Bacteria. *J. Med. Chem.* **2017**, *60*, 3221−3240.

(17) Jin, Z.; El-Deiry, W. S. Overview of cell death signaling pathways. *Cancer Biol. Ther.* **2005**, *4*, 147−171.

(18) Matthews, H. K.; Bertoli, C.; de Bruin, R. A. M. Cell cycle control in cancer. *Nat. Rev. Mol. Cell Biol.* **2022**, *23*, 74−88.

(19) Banerjee, S.; Chakravarty, A. R. Metal Complexes of Curcumin for Cellular Imaging, Targeting, and Photo-induced Anticancer Activity. *Acc. Chem. Res.* **2015**, *48*, 2075−2083.

(20) Huang, C.; Liang, C.; Sadhukhan, T.; Banerjee, S.; Fan, Z.; Li, T.; Zhu, Z.; Zhang, P.; Raghavachari, K.; Huang, H. In-vitro and In-vivo Photocatalytic Cancer Therapy with Bio-compatible Iridium(III) Photocatalysts. *Angew. Chem., Int. Ed.* **2021**, *60*, 9474−9479.

(21) Huang, H.; Banerjee, S.; Qiu, K.; Zhang, P.; Blacque, O.; Malcomson, T.; Paterson, M. J.; Clarkson, G. J.; Staniforth, M.; Stavros, V. G.; Gasser, G.; Chao, H.; Sadler, P. J. Targeted photoredox catalysis in cancer cells. *Nat. Chem.* **2019**, *11*, 1041−1048.

(22) Fan, Z.; Xie, J.; Sadhukhan, T.; Liang, C.; Huang, C.; Li, W.; Li, T.; Zhang, P.; Banerjee, S.; Raghavachari, K.; Huang, H. Highly Efficient Ir (III)-Coumarin Photo-Redox Catalyst for Synergetic Multi-Mode Cancer Photo-Therapy. *Chem.—Eur. J.* **2022**, *28*, No. e202103346.

(23) Navas, L. E.; Carnero, A. NAD^+ metabolism, stemness, the immune response, and cancer. *Signal Transduction Targeted Ther.* **2021**, *6*, 2.

(24) Tyagi, K.; Dixit, T.; Venkatesh, V. Recent advances in catalytic anticancer drugs: Mechanistic investigations and future prospects. *Inorg. Chim. Acta* **2022**, *533*, No. 120754.

(25) Swaminathan, S.; Deepak, J. R.; Karvembu, R. Interweaving catalysis and cancer using Ru- and Os-arene complexes to alter cellular redox state: A structure-activity relationship (SAR) review. *Coord. Chem. Rev.* **2023**, *491*, No. 215230.

(26) Banerjee, S.; Sadler, P. J. Transfer hydrogenation catalysis in cells. *RSC Chem. Biol.* **2021**, *2*, 12−29.

(27) Fan, Z.; Huang, J.; Huang, H.; Banerjee, S. Metal-Based Catalytic Drug Development for Next-Generation Cancer Therapy. *ChemMedChem.* **2021**, *16*, 2480−2486.
(28) Soldevila-Barreda, J. J.; Metzler-Nolte, N. Intracellular catalysis with selected metal complexes and metallic nanoparticles: advances toward the development of catalytic metallodrugs. *Chem. Rev.* **2019**, *119*, 829−869.
(29) Soldevila-Barreda, J. J.; Sadler, P. J. Approaches to the design of catalytic metallodrugs. *Curr. Opin. Chem. Biol.* **2015**, *25*, 172−183.
(30) Li, Y.-L.; Li, A.-J.; Huang, S.-L.; Vittal, J. J.; Yang, G.-Y. Polypyridyl Ru(II) or cyclometalated Ir(III) functionalized architectures for photocatalysis. *Chem. Soc. Rev.* **2023**, *52*, 4725−4754.
(31) DiLuzio, S.; Connell, T. U.; Mdluli, V.; Kowalewski, J. F.; Bernhard, S. Understanding Ir(III) Photocatalyst Structure−Activity Relationships: A Highly Parallelized Study of Light-Driven Metal Reduction Processes. *J. Am. Chem. Soc.* **2022**, *144*, 1431−1444.
(32) Schmid, L.; Glaser, F.; Schaer, R.; Wenger, O. S. High Triplet Energy Iridium(III) Isocyanoborato Complex for Photochemical Upconversion, Photoredox and Energy Transfer Catalysis. *J. Am. Chem. Soc.* **2022**, *144*, 963−976.
(33) Deng, Z.; Li, H.; Chen, S.; Wang, Na; Liu, G.; Liu, D.; Ou, W.; Xu, F.; Wang, X.; Lei, D.; Lo, P.-C.; Li, Y. Y.; Lu, J.; Yang, M.; He, M.-L.; Zhu, G. Near-infrared-activated anticancer platinum(IV) complexes directly photooxidize biomolecules in an oxygen-independent manner. *Nat. Chem.* **2023**, *15*, 930−939.
(34) (a) Karges, J.; Heinemann, F.; Jakubaszek, M.; Maschietto, F.; Subecz, C.; Dotou, M.; Vinck, R.; Blacque, O.; Tharaud, M.; Goud, B.; Zahínos, E. V.; Spingler, B.; Ciofini, I.; Gasser, G. Rationally Designed Long-Wavelength Absorbing Ru(II) Polypyridyl Complexes as Photosensitizers for Photodynamic Therapy. *J. Am. Chem. Soc.* **2020**, *142*, 6578−6587. (b) Notaro, A.; Gasser, G. Monomeric and dimeric coordinatively saturated and substitutionally inert Ru(II) polypyridyl complexes as anticancer drug candidates. *Chem. Soc. Rev.* **2017**, *46*, 7317−7337.
(35) Heinemann, F.; Karges, J.; Gasser, G. Critical Overview of the Use of Ru(II) Polypyridyl Complexes as Photosensitizers in One-Photon and Two-Photon Photodynamic Therapy. *Acc. Chem. Res.* **2017**, *50*, 2727−2736.
(36) Karges, J.; Kuang, S.; Maschietto, F.; Blacque, O.; Ciofini, I.; Chao, H.; Gasser, G. Rationally designed ruthenium complexes for 1- and 2-photon photodynamic therapy. *Nat. Commun.* **2020**, *11*, 3262.
(37) Howerton, B. S.; Heidary, D. K.; Glazer, E. C. Strained Ruthenium Complexes Are Potent Light-Activated Anticancer Agents. *J. Am. Chem. Soc.* **2012**, *134*, 8324−8327.
(38) Wachter, E.; Heidary, D. K.; Howerton, B. S.; Parkin, S.; Glazer, E. C. Light-activated ruthenium complexes photobind DNA and are cytotoxic in the photodynamic therapy window. *Chem. Commun.* **2012**, *48*, 9649−9651.
(39) Monro, S.; Colón, K. L.; Yin, H.; Roque, J., III; Konda, P.; Gujar, S.; Thummel, R. P.; Lilge, L.; Cameron, C. G.; McFarland, S. A. Transition Metal Complexes and Photodynamic Therapy from a Tumor-Centered Approach: Challenges, Opportunities, and Highlights from the Development of TLD1433. *Chem. Rev.* **2019**, *119*, 797−828.
(40) Bonnet, S. Why develop photoactivated chemotherapy? *Dalton Trans.* **2018**, *47*, 10330−10343.
(41) Shi, G.; Monro, S.; Hennigar, R.; Colpitts, J.; Fong, J.; Kasimova, K.; Yin, H.; DeCoste, R.; Spencer, C.; Chamberlain, L.; Mandel, A.; Lilge, L.; McFarland, S. A. Ru(II) dyads derived from α-oligothiophenes: A new class of potent and versatile photosensitizers for PDT. *Coord. Chem. Rev.* **2015**, *282*−*283*, 127−138.
(42) Lifshits, L. M.; Roque, J. A. III; Konda, P.; Monro, S.; Cole, H. D.; von Dohlen, D.; Kim, S.; Deep, G.; Thummel, R. P.; Cameron, C. G.; Gujar, S.; McFarland, S. A. Near-infrared absorbing Ru(II) complexes act as immunoprotective photodynamic therapy (PDT) agents against aggressive melanoma. *Chem. Sci.* **2020**, *11*, 11740−11762.
(43) Bonnet, S. Ruthenium-Based Photoactivated Chemotherapy. *J. Am. Chem. Soc.* **2023**, *145*, 23397−23415.
(44) Mari, C.; Pierroz, V.; Ferrari, S.; Gasser, G. Combination of Ru(II) complexes and light: new frontiers in cancer therapy. *Chem. Sci.* **2015**, *6*, 2660−2686.
(45) Heinemann, F.; Karges, J.; Gilles, G. Critical Overview of the Use of Ru(II) Polypyridyl Complexes as Photosensitizers in One-Photon and Two-Photon Photodynamic Therapy. *Acc. Chem. Res.* **2017**, *50*, 2727−2736.
(46) Mari, C.; Pierroz, V.; Rubbiani, R.; Patra, M.; Hess, J.; Spingler, B.; Oehninger, L.; Schur, J.; Ott, I.; Salassa, L.; Ferrari, S.; Gasser, G. DNA Intercalating Ru(II) Polypyridyl Complexes as Effective Photosensitizers in Photodynamic Therapy. *Chem.—Eur. J.* **2014**, *20*, 14421−14436.
(47) Paul, S.; Kundu, P.; Kondaiah, P.; Chakravarty, A. R. BODIPY-Ruthenium(II) Bis-Terpyridine Complexes for Cellular Imaging and Type-I/-II Photodynamic Therapy. *Inorg. Chem.* **2021**, *60*, 16178−16193.
(48) Li, J.; Zeng, L.; Xiong, K.; Rees, T. W.; Jin, C.; Wu, W.; Chen, Yu.; Jia, L.; Chao, H. A biotinylated ruthenium(II) photosensitizer for tumor-targeted two-photon photodynamic therapy. *Chem. Commun.* **2019**, *55*, 10972−10975.
(49) Steinke, S. J.; Gupta, S.; Piechota, E. J.; Moore, C. E.; Kodanko, J. J.; Turro, C. Photocytotoxicity and photoinduced phosphine ligand exchange in a Ru(II) polypyridyl complex. *Chem. Sci.* **2022**, *13*, 1933−1945.
(50) Chen, Q.; Cuello-Garibo, J. A.; Bretin, L.; Zhang, L.; Ramu, V.; Aydar, Y.; Batsiun, Y.; Bronkhorst, S.; Husiev, Y.; Beztsinna, N.; Chen, L.; Zhou, X. Q.; Schmidt, C.; Ott, I.; Jager, M. J.; Brouwer, A. M.; Snaar-Jagalska, B. E.; Bonnet, S. Photosubstitution in a trisheteroleptic ruthenium complex inhibits conjunctival melanoma growth in a zebrafish orthotopic xenograft model. *Chem. Sci.* **2022**, *13*, 6899−6919.
(51) Havrylyuk, D.; Hachey, A. C.; Fenton, A.; Heidary, D. K.; Glazer, E. C. Ru(II) photocages enable precise control over enzyme activity with red light. *Nat. Commun.* **2022**, *13*, 3636.
(52) Gandioso, A.; Izquierdo-García, E.; Mesdom, P.; Arnoux, P.; Demeubayeva, N.; Burckel, P.; Saubaméa, B.; Bosch, M.; Frochot, C.; Marchán, V.; Gasser, G. Ru(II)-Cyanine Complexes as Promising Photodynamic Photosensitizers for the Treatment of Hypoxic Tumours with Highly Penetrating 770 nm Near-Infrared Light. *Chem.—Eur. J.* **2023**, *29*, No. e202301742.
(53) Pierroz, V.; Rubbiani, R.; Gentili, C.; Patra, M.; Mari, C.; Gasser, G.; Ferrari, S. Dual mode of cell death upon the photo-irradiation of a Ru(II) polypyridyl complex in interphase or mitosis. *Chem. Sci.* **2016**, *7*, 6115−6124.
(54) Pozza, M. D.; Mesdom, P.; Abdullrahman, A.; Otoya, T. D. P.; Arnoux, P.; Frochot, C.; Niogret, G.; Saubaméa, B.; Burckel, P.; Hall, J. P.; Hollenstein, M.; Cardin, C. J.; Gasser, G. Increasing the π-Expansive Ligands in Ruthenium(II) Polypyridyl Complexes: Synthesis, Characterization, and Biological Evaluation for Photodynamic Therapy Applications. *Inorg. Chem.* **2023**, *62*, 18510−18523.
(55) Mariappan, M.; Maiya, B. G. Effects of Anthracene and Pyrene Units on the Interactions of Novel Polypyridylruthenium(II) Mixed-Ligand Complexes with DNA. *Eur. J. Inorg. Chem.* **2005**, *2005*, 2164−2173.
(56) Tan, L.-F.; Chao, H.; Li, H.; Liu, Y.-J.; Sun, B.; Wei, W.; Ji, L.-N. J. Synthesis, characterization, DNA-binding and photocleavage studies of $[Ru(bpy)_2(PPIP)]^{2+}$ and $[Ru(phen)_2(PPIP)]^{2+}$. *Inorg. Biochem.* **2005**, *99*, 513−520.
(57) Huang, H.; Zhang, P.; Chen, Y.; Qiu, K.; Jin, C.; Jia, L.; Chao, H. Synthesis, characterization and biological evaluation of labile intercalative ruthenium(II) complexes for anticancer drug screening. *Dalton Trans.* **2016**, *45*, 13135−13145.
(58) Mitchell, R. J.; Kriger, S. M.; Fenton, A. D.; Havrylyuk, D.; Pandeya, A.; Sun, Y.; Smith, T.; DeRouchey, J. E.; Unrine, J. M.; Oza, V.; Blackburn, J. S.; Wei, Y.; Heidary, D. K.; Glazer, E. C. A mono adduct generating Ru(II) complex induces ribosome biogenesis stress and is a molecular mimic of phenanthriplatin. *RSC Chem. Biol.* **2023**, *4*, 344−353.

https://doi.org/10.1021/acs.inorgchem.4c00650
Inorg. Chem. 2024, 63, 7493−7503

(59) Yu, H.-j.; Liu, J.-p.; Hao, Z.-f.; He, J.; Sun, M.; Hu, S.; Yu, L.; Chao, H. Synthesis, characterization and biological evaluation of ruthenium(II) complexes $[Ru(dtzp)(dppz)Cl]^{+}$ and $[Ru(dtzp)(dppz)CH_3CN]^{2+}$ for photodynamic therapy. *Dyes Pigm.* **2017**, *136*, 416−426.
(60) Rilak, A.; Bratsos, I.; Zangrando, E.; Kljun, J.; Turel, I.; Bugarčič, Ž. D.; Alessio, E. New Water-Soluble Ruthenium(II) Terpyridine Complexes for Anticancer Activity: Synthesis, Characterization, Activation Kinetics, and Interaction with Guanine Derivatives. *Inorg. Chem.* **2014**, *53*, 6113−6126.
(61) Catalano, V. J.; Craig, T. J. Monometallic and Dimetallic Ruthenium(II)−Terpyridine Complexes Employing the Tetradentate Ligands Dipyridylpyrazolyl, Dipyridyloxadiazole, and Their Dimethyl Derivatives. *Inorg. Chem.* **2003**, *42*, 321−334.
(62) Puckett, C. A.; Barton, J. K. Methods to explore cellular uptake of ruthenium complexes. *J. Am. Chem. Soc.* **2007**, *129*, 46−47.
(63) Huang, H.; Zhang, P.; Chen, H.; Ji, L.; Chao, H. Comparison between Polypyridyl and Cyclometalated Ruthenium(II) Complexes: Anticancer Activities against 2D and 3D Cancer Models. *Chem.—Eur. J.* **2015**, *21*, 715−725.
(64) Fetzer, L.; Boff, B.; Ali, M.; Xiangjun, M.; Collin, J.-P.; Sirlin, C.; Gaiddon, C.; Pfeffer, M. Library of Second-Generation Cycloruthenate Compounds and Evaluation of Their Biological Properties as Potential Anticancer Drugs: Passing the Nanomolar Barrier. *Dalton Trans.* **2011**, *40*, 8869−8878.
(65) Ghosh, G.; Colón, K. L.; Fuller, A.; Sainuddin, T.; Bradner, E.; McCain, J.; Monro, S. M. A.; Yin, H.; Hetu, M. W.; Cameron, C. G.; McFarland, S. A. Cyclometalated Ruthenium(II) Complexes Derived from αOligothiophenes as Highly Selective Cytotoxic or Photocytotoxic Agents. *Inorg. Chem.* **2018**, *57*, 7694−7712.
(66) Bera, A.; Gautam, S.; Sahoo, S.; Pal, A. K.; Kondaiah, P.; Chakravarty, A. R. Red light active Pt(IV)−BODIPY prodrug as a mitochondria and endoplasmic reticulum targeted chemo-PDT agent. *RSC Med. Chem.* **2022**, *13*, 1526−1539.
(67) Frisch, M. J.; Trucks, G. W.; Schlegel, H. B.; Scuseria, G. E.; Robb; Cheeseman, J. R; Scalmani, G.; Barone, S. V.; Petersson, G. A.; Nakatsuji, H.; Li, X. *Gaussian 16*, Revision A.03; Gaussian Inc.: Wallingford, CT, 2016.
(68) Yu, L.; Lee, K.-W.; Zhao, Y.-Q.; Xu, Y.; Zhou, Y.; Li, M.; Kim, J. S. Metal Modulation: An Effortless Tactic for Refining Photoredox Catalysis in Living Cells. *Inorg.Chem.* **2023**, *62*, 18767−18778.
(69) Yadav, A. K.; Singh, V.; Kushwaha, R.; Dolui, D.; Rai, R.; Dhar, P.; Dutta, A.; Koch, B.; Banerjee, S. Polypyridyl Co(II)-Curcumin Complexes as Photo-activated Anticancer and Antibacterial Agents. *ChemBioChem* **2023**, *24*, No. e202300033.
(70) Feng, T.; Tang, Z.; Karges, J.; Shen, J.; Jin, C.; Chen, Y.; Pan, Y.; He, Y.; Ji, L.; Chao, H. Exosome camouflaged coordination-assembled Iridium(III) photosensitizers for apoptosis-autophagy-ferroptosis induced combination therapy against melanoma. *Biomater.* **2023**, *301*, No. 122212.
(71) Wang, Y.; Mesdom, P.; Purkait, K.; Saubaméa, B.; Burckel, P.; Arnoux, P.; Frochot, C.; Cariou, K.; Rossel, T.; Gasser, G. Ru(II)/Os(II)-based carbonic anhydrase inhibitors as photodynamic therapy photosensitizers for the treatment of hypoxic tumours. *Chem. Sci.* **2023**, *14*, 11749−11760.
(72) Zeng, L.; Chen, Y.; Liu, J.; Huang, H.; Guan, R.; Ji, L.; Chao, H. Ruthenium(II) Complexes with 2-Phenylimidazo[4,5-f][1,10]-phenanthroline Derivatives that Strongly Combat Cisplatin-Resistant Tumor Cells. *Sci. Rep.* **2016**, *6*, 19449.
(73) Liu, Z.; Habtemariam, A.; Pizarro, A. M.; Clarkson, G. J.; Sadler, P. J. Organometallic Iridium(III) Cyclopentadienyl Anticancer Complexes Containing C,N-Chelating Ligands. *Organometallics* **2011**, *30*, 4702−4710.
(74) Swathantraiah, J. G.; Srinivasa, S. M.; Motatis, A. K. B.; Uttarkar, A.; Bettaswamygowda, S.; Thimmaiah, S. B.; Niranjan, V.; Rangappa, S.; Subbegowda, R. K.; Ramegowda, T. N. Novel 1,2,5-Trisubstituted Benzimidazoles Potentiate Apoptosis by Mitochondrial Dysfunction in Panel of Cancer Cells. *ACS Omega* **2022**, *7*, 46955−46971.
(75) Ali, I.; Lone, M. N.; Aboul-Enein, H. Y. Imidazoles as potential anticancer agents. *Med. Chem. Commun.* **2017**, *8*, 1742−1773.
(76) Huang, H.; Zhang, P.; Chen, Y.; Ji, L.; Chao, H. Labile ruthenium(II) complexes with extended phenyl-substituted terpyridyl ligands: synthesis, aquation and anticancer evaluation. *Dalton Trans.* **2015**, *44*, 15602−15610.
(77) Peña, B.; David, A.; Pavani, C.; Baptista, M. S.; Pellois, J. P.; Turro, C.; Dunbar, K. R. Cytotoxicity Studies of Cyclometallated Ruthenium(II) Compounds: New Applications for Ruthenium Dyes. *Organometallics* **2014**, *33*, 1100−1103.
(78) Roy, S.; Colombo, E.; Vinck, R.; Mari, C.; Rubbiani, R.; Patra, M.; Gasser, G. Increased Lipophilicity of Halogenated Ruthenium(II) Polypyridyl Complexes Leads to Decreased Phototoxicity in vitro when Used as Photosensitizers for Photodynamic Therapy. *ChemBioChem.* **2020**, *21*, 2966−2973.
(79) Frei, A.; Rubbiani, R.; Tubafard, S.; Blacque, O.; Anstaett, P.; Felgentrager, A.; Maisch, T.; Spiccia, L.; Gasser, G. Synthesis, Characterization, and Biological Evaluation of New Ru(II) Polypyridyl Photosensitizers for Photodynamic Therapy. *J. Med. Chem.* **2014**, *57*, 7280−7292.
(80) Mandal, A.; Rai, R.; Saha, S.; Kushwaha, R.; Wei, L.; Gogoi, H.; Mandal, A. A.; Yadav, A. K.; Huang, H.; Dutta, A.; Dhar, P.; Banerjee, S. Polypyridyl-based Co(III) complexes of vitamin B_6 Schiff base for photoactivated antibacterial therapy. *Dalton Trans.* **2023**, *52*, 17562−17572.
(81) McFarland, S. A.; Mandel, A.; Dumoulin-White, R.; Gasser, G. Metal-based photosensitizers for photodynamic therapy: the future of multimodal oncology? *Curr. Opin. Chem. Biol.* **2020**, *56*, 23−27.
(82) Rees, T. W.; Ho, P.; Hess, J. Recent Advances in Metal Complexes for Antimicrobial Photodynamic Therapy. *ChemBioChem* **2023**, *24*, No. e202200796.
(83) Arora, K.; Herroon, M.; Al-Afyouni, M. H.; Toupin, N. P.; Rohrabaugh, T. N.; Loftus, L. M.; Podgorski, I.; Turro, C.; Kodanko, J. J. Catch and Release Photosensitizers: Combining Dual-Action Ru Complexes with Protease Inactivation for Targeting Invasive Cancers. *J. Am. Chem. Soc.* **2018**, *140*, 14367−14380.
(84) Zhang, L.; Wang, P.; Zhou, X.-Q.; Bretin, L.; Zeng, X.; Husiev, Y.; Polanco, E. A.; Zhao, G.; Wijaya, L. S.; Biver, T.; Le Dévédec, S. E.; Sun, W.; Bonnet, S. Cyclic Ruthenium-Peptide Conjugates as Integrin-Targeting Phototherapeutic Prodrugs for the Treatment of Brain Tumors. *J. Am. Chem. Soc.* **2023**, *145*, 1496−14980.
(85) Bera, A.; Nepalia, A.; Upadhyay, A.; Saini, D. K.; Chakravarty, A. R. Biotin and boron-dipyrromethene-tagged platinum(IV) prodrug for cellular imaging and mito-targeted photocytotoxicity in red light. *Dalton Trans.* **2023**, *52*, 13339−13350.
(86) Ouyang, C.; Chen, L.; Rees, T. W.; Chen, Y.; Liu, J. K.; Ji, L. N.; Long, J. G.; Chao, H. A mitochondria-targeting hetero-binuclear Ir(III)−Pt(II) complex induces necrosis in cisplatin-resistant tumor cells. *Chem. Commun.* **2018**, *54*, 6268−6271.
(87) Bera, A.; Gautam, S.; Raza, M. K.; Kondaiah, P.; Chakravarty, A. R. Oxoplatin-B, a cisplatin-based platinum(IV) complex with photoactive BODIPY for mitochondria specific "chemo-PDT" activity. *J. Inorg. Biochem.* **2021**, *223*, No. 111526.

https://doi.org/10.1021/acs.inorgchem.4c00650
Inorg. Chem. 2024, 63, 7493−7503